

The Relevance of Measurement Systems Analysis

A Procter & Gamble Case Study on MSA Methodology and Applications

DATE

**OCTOBER
10 AND 12**

TIME

**16:00 CET,
10 am EST**



**CHRISTIAN
NEU**

Scientist
Procter & Gamble



**JERRY
FISH**

Systems Engineer
JMP



**JASON
WIGGINS**

Senior Systems
Engineer
JMP

[Register now](#)

Monitoring DNA Hybridization with Organic Electrochemical Transistors Functionalized with Polydopamine

Matteo Sensi,* Giulio Migatti, Valerio Beni, Tommaso Marchesi D'Alvise, Tanja Weil, Marcello Berto, Pierpaolo Greco, Carol Imbriano, Fabio Biscarini, and Carlo Augusto Bortolotti

Organic electrochemical transistors (OECTs) are finding widespread application in biosensing, thanks to their high sensitivity, broad dynamic range, and low limit of detection. An OECT biosensor requires the immobilization of a biorecognition probe on the gate, or else on the channel, through several, often lengthy, chemical steps. In this work, a fast and straightforward way to functionalize the carbon gate of a fully screen-printed OECT by means of a polydopamine (PDA) film is presented. By chemical immobilization of an amine-terminated single-stranded oligonucleotide, containing the HSP70 promoter CCAAT sequence, on the PDA film, the detection of the complementary DNA strand is demonstrated. Furthermore, the specificity of the developed genosensor is assessed by comparing its response to the fully complementary strand with the one to partially complementary and noncomplementary oligonucleotides. The developed sensor shows a theoretical limit of detection (LOD) of 100×10^{-15} M and a dynamic range over four orders of magnitude.

1. Introduction

Label-free biosensors based on electrolyte-gated organic transistors (EGOTs) are emerging technologies^[1] for the detection of a wide range of targets, including neurotransmitters,^[2,3] proteins,^[4–7] antibodies,^[8] oligonucleotides,^[10,9] and even viruses.^[11] EGOTs encompass electrolyte-gated organic field-effect transistors (EGOFETs) and organic electrochemical transistors (OECTs). The latter can be operated either in faradic or non-faradic regimes, depending on whether the modulation of the channel conductance is achieved by faradic processes at the gate, caused by the presence of redox-active molecules on the gate/channel or in the electrolyte solution,^[12–14] or rather by capacitive charging of the ionic double layer at the gate electrode, which causes ions to penetrate in the channel.^[15] In OECTs, source and drain electrodes are connected by a p- or n-type organic semiconductor, in contact with a third electrode, called gate, through an electrolyte. The current in the channel, generated by applying a drain–source voltage (V_{DS}), is modulated by a second voltage applied between the source and gate electrodes (V_{GS}). The modulation of the channel strongly depends on the gate and channel materials, but also on the gate or channel functionalization with the sensing probe and the electrolyte composition.

In recent years, the potentiality of additive manufacturing, and more specifically screen-printing, for the large-scale manufacturing of OECTs for sensing^[13,16,17] and digital circuits applications^[18,19] has been demonstrated. In literature, examples of oligonucleotides detection by means of OECTs^[20,21,9] and EGOFETs^[22,23] can be found; the key to the sensor performance is the reliable immobilization of a specific oligonucleotide probe on the gate electrode. Several approaches have been reported to perform the immobilization of the probe including the use of thiol-based self-assembled monolayers,^[24] hydrogels,^[17,22,25] carbon-based matrices,^[26] and proteins.^[27] Most of the cited methods require a “blocking step” in which anti-fouling molecular monolayers or proteins are added to avoid/minimize the non-specific


M. Sensi, G. Migatti, M. Berto, P. Greco, C. Imbriano, F. Biscarini, C. A. Bortolotti

Department of Life Sciences
 Università di Modena e Reggio Emilia
 via Campi 103, Modena 41125, Italy
 E-mail: matteo.sensi@unimore.it

V. Beni
 Department of Smart Hardware
 Bio- & Organic Electronics Unit
 RISE AB
 Research Institute of Sweden
 Bredgatan 33, Norrköping 602 21, Sweden

T. M. D'Alvise, T. Weil
 Max Planck Institute for Polymer Research
 Ackermannweg 10, Mainz 55128, Germany

P. Greco, F. Biscarini
 Center for Translational Neurophysiology-Istituto Italiano di Tecnologia
 Via Fossato di Mortara 17–19, Ferrara 44121, Italy

 The ORCID identification number(s) for the author(s) of this article can be found under <https://doi.org/10.1002/mame.202100880>

© 2022 The Authors. Macromolecular Materials and Engineering published by Wiley-VCH GmbH This is an open access article under the terms of the Creative Commons Attribution License, which permits use, distribution and reproduction in any medium, provided the original work is properly cited.

DOI: 10.1002/mame.202100880

adsorption of biomolecules (i.e., specific and/or unspecific DNA strands) onto the gate.

An alternative immobilization strategy, which has been previously reported for electrochemical sensing^[28] but never for EGOTs, takes advantage of the peculiar properties of polydopamine (PDA). PDA is a bioinspired, highly cross-linked polymer that is formed by the polymerization of the naturally occurring neurotransmitter dopamine.^[29] Polymerization and film formation proceeds in a fast and straightforward fashion by simple air-induced oxidation on various surfaces.^[29] Although the exact structure of PDA has not yet been completely clarified,^[30,31] various functionalities are known to be formed during the polymerization process such as catechols, quinones, and indoles, which allow straightforward functionalization.^[32] In particular, the catechol and quinone groups on the film surface can interact in a covalent as well as noncovalent fashion with the molecules and proteins of interest through hydrogen bonds, Michael's addition, and Schiff's base chemistry and pi-stacking. For example, Michael additions or Schiff base reactions between the quinone surface groups of PDA and amino groups^[28,33] or thiol groups,^[34–36] introduced at the 5' or 3' end of oligonucleotide probes, have been reported demonstrating an outstanding functionalization density.^[37] Therefore, the use of PDA can be considered a promising gate functionalization strategy for electrolyte-gated organic transistors.

In this work, we exploit the properties of PDA to easily functionalize, via Michael's addition or Schiff base chemistry, the carbon gate of fully printed OECTs with an oligonucleotide probe, for the development of a genosensor for the detection of the reverse strand of an oligonucleotide containing the HSP70 promoter CCAAT sequence. The CCAAT box represents the binding site specifically recognized by the transcription factor NF- κ B, whose overexpression has been associated with cancer progression and aggressiveness.^[38,39] Assessment of the developed genosensor was performed by evaluating its ability to hybridize and selectively detect its reverse complementary sequence and to form double-stranded DNA (dsDNA). By exposing the biosensor to fully complementary DNA, and by performing control experiments with mismatch-bearing and noncomplementary strands, we demonstrate the potential use of the device not only for the detection of oligonucleotides at low concentrations (theoretical LOD $\approx 100 \times 10^{-15}$ M) but also for investigating the specificity of biorecognition and fundamental aspects of the hybridization processes.

2. Results and Discussion

The device described in this work is a flexible planar organic electrochemical transistor genosensor printed on PET, consisting of a PEDOT:PSS channel and a coplanar carbon gate electrode.^[13,16] To facilitate the immobilization of an amino-modified oligonucleotide probe (see **Figure 1**, panels a and b), the gate electrode was modified with a PDA film.^[40] More specifically, we exploited the ability of dopamine (DA) to spontaneously polymerize on various surfaces, i.e., metals or polymers, from buffered solutions.^[29] In the work reported herein, we modified the gate electrode by drop-casting 10 μ L of 1 mg mL⁻¹ DA solution in 1 \times phosphate-buffered saline (PBS) buffer at pH 7.4 for 24 h at RT. As shown in **Figure 1c**, the formation of the PDA film was

monitored by cyclic voltammetry (CV), connecting the gate as the working electrode. The formation of the PDA film was detected by the appearance of two redox peaks/shoulders usually associated with catechol oxidation and quinones reduction,^[41,42] at 140 mV and 50 mV versus Ag/AgCl, respectively. PDA film formation was also monitored by faradaic electrochemical impedance spectroscopy (EIS), where we observed an increase in the charge transfer resistance (R_{ct}) between the $K_3[Fe(CN)_6]$ redox probe and the gate electrode upon film formation (**Figure S1**, Supporting Information).

We then immobilized a single-stranded oligonucleotide probe on the PDA-modified gate. A 25-base long oligonucleotide was selected featuring an amino group at the 5' end of a C6-spacer; its full sequence is reported in the materials and methods section. We will refer to this oligonucleotide and its complementary ssDNA strand (lacking the C6-spacer as well as the terminal amino group) as the "probe" and the "fc-target" (full-complementary target), respectively.

Grafting of the DNA probe onto the PDA film has been accomplished by the formation of a new covalent bond between its 5' amino-terminal group on DNA and the PDA exposing quinone groups, that could proceed either through Michael addition and/or through Schiff base reaction.^[28,29,43] As a result of the reaction, the PDA film presents catechol groups, and a bond is formed with the amino-terminal group of the oligonucleotide. More specifically, we covered the gate electrode with 10 μ L of a 10×10^{-6} M probe solution in 1 \times PBS buffer, at pH 8 for 4 h at RT. To monitor DNA binding, we measured the transfer characteristics of the device by applying $V_{DS} = -0.2$ V and V_{GS} from -0.2 V to 0.4 V, and cyclic voltammetry, connecting the gate as a working electrode, in 1 \times PBS buffer at pH 7.4. In **Figure 2a** we compare the transfer characteristics for OECTs with bare carbon gate (black line), carbon gate–PDA (red line), and carbon gate–PDA–DNA modified gate (blue line). The carbon gate does not modulate the transfer curve, since it is necessary to extend the V_{GS} range to 2 V to obtain a significant modulation due to redox reactions taking place at the electrode surface, as previously reported.^[13] Upon gate functionalization, we observe a slight modulation (see **Figure S5**, Supporting Information). It is however apparent that the deposition of PDA and then the binding of the probe both induce a decrease in the I_{DS} current. The absence (or modest) of V_{GS} modulation suggests that we are mostly observing the response due to the change of channel conductivity because of the change of the electrochemical potential of the electrolyte, due to the gate functionalization.^[45]

To gain a better insight into the results of the transfer experiment, the gate currents (I_{GS}) were also plotted and analyzed. The absence of any redox peak in a wide range of voltages makes the carbon gate suitable to study the reactivity of redox enzymes^[46] and polymers, like PDA. Whereas no redox reactions take place at the bare carbon gate, in the used V_{GS} window, in the case of the PDA modified gate two broad peaks/shoulders around 0.2 and 0.1 V were recorded, indicating the presence of redox processes. These redox signals disappeared when DNA was immobilized on the carbon/PDA gate (**Figure 2b**, blue line). Since DNA is likely to bind to the quinones on the PDA film, these observations confirm the attribution of the redox signal in the I_{GS} to the catechol group's oxidation in the PDA film, and they also support the successful covalent immobilization of the DNA strand. In addition,

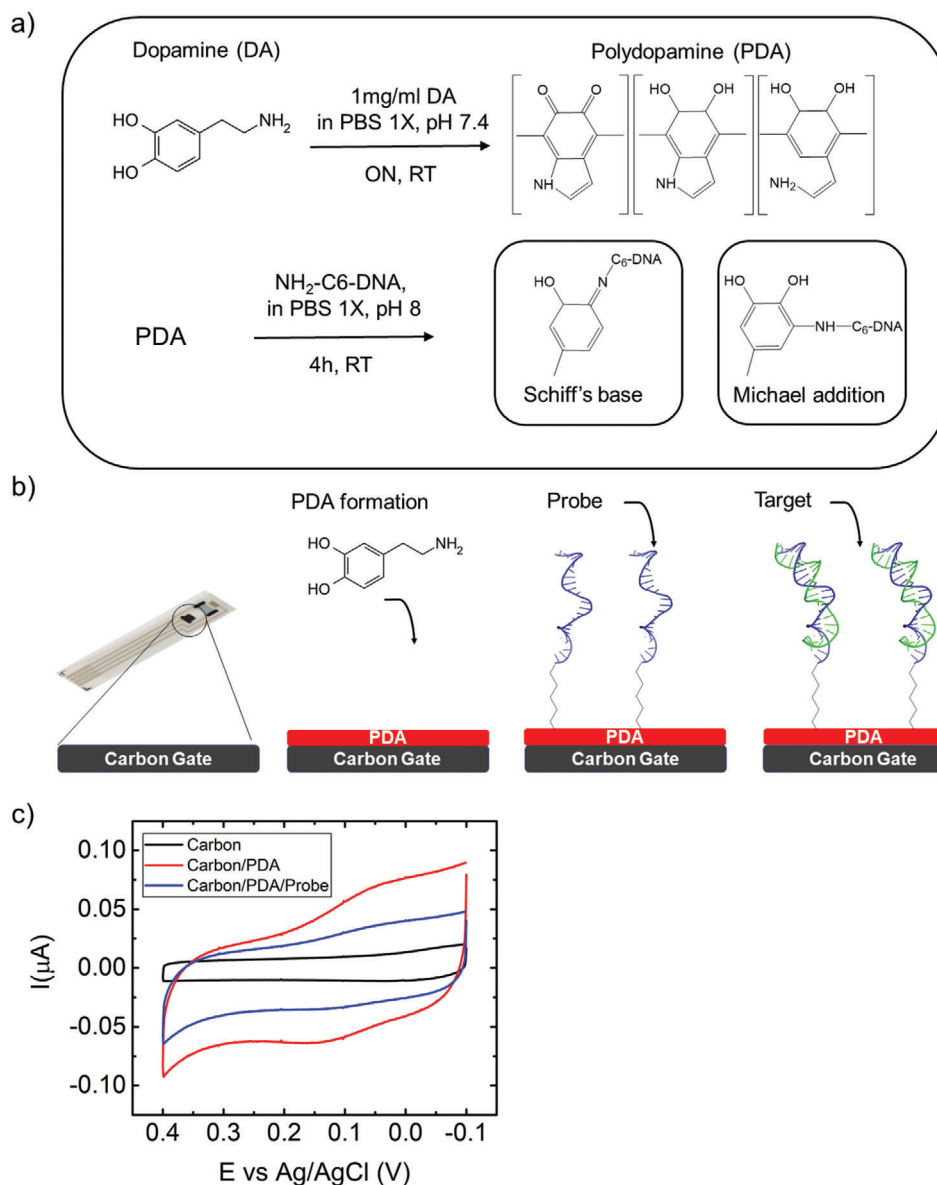


Figure 1. Polydopamine film deposition. a) PDA film formation and probe immobilization reaction scheme. PDA is a highly crosslinked structurally complex material and only some of the possible structural components are shown; for a more in-depth discussion about PDA structure see for example refs. #0028,31, and #0041. b) Schematic representation of the OECT and the steps of carbon gate functionalization by PDA, probe, and detection of fc-target (the DNA 3D structure was taken from the PDB file 4WAL). c) Cyclic voltammetry of the carbon gate before (black) and after (red) deposition of PDA by drop-casting and after immobilization of the probe sequence (blue). The CVs were recorded in PBS 1X, at pH 7.4 and 50 mV s⁻¹. RT, room temperature; ON, overnight.

also the CVs reported in Figure 2b support these experimental findings. The presence of the PDA redox processes has a direct effect on the drain-source current, which can be observed by examining the first derivative of the transfer curves, viz. the transconductance (Figure 2c). The transconductance increases after deposition of PDA on the carbon gate (red line), exhibiting a marked shoulder at +140 mV, viz. the potential corresponding to the peak in Figures 1c and 2b. The shoulder then disappears after immobilization of the DNA probe on the PDA film, consistently with what was observed in the CVs (Figure 1c) and in the I_{GS} versus V_{GS} curves (Figure 2b). The functionalized device shows good sta-

bility over time, exhibiting a change of 1.5% of I_{DS} current at $V_{GS} = 0.4$ V after 15 days at room temperature in a petri dish (Figure S7, Supporting Information).

To assess the hybridization between the probe and the complementary strand, we exposed the functionalized device to 1× PBS solutions containing increasing concentrations, ranging from 1×10^{-12} M to 100×10^{-9} M of the fc-target oligonucleotide, followed by recording, in situ, of the transfer curves. After each change of solution, the transfer curves were recorded continuously for 15 min until stabilization of the I_{DS} current was observed. A V_{GS} window between -0.2 V to 0.4 V and a fixed V_{DS} of

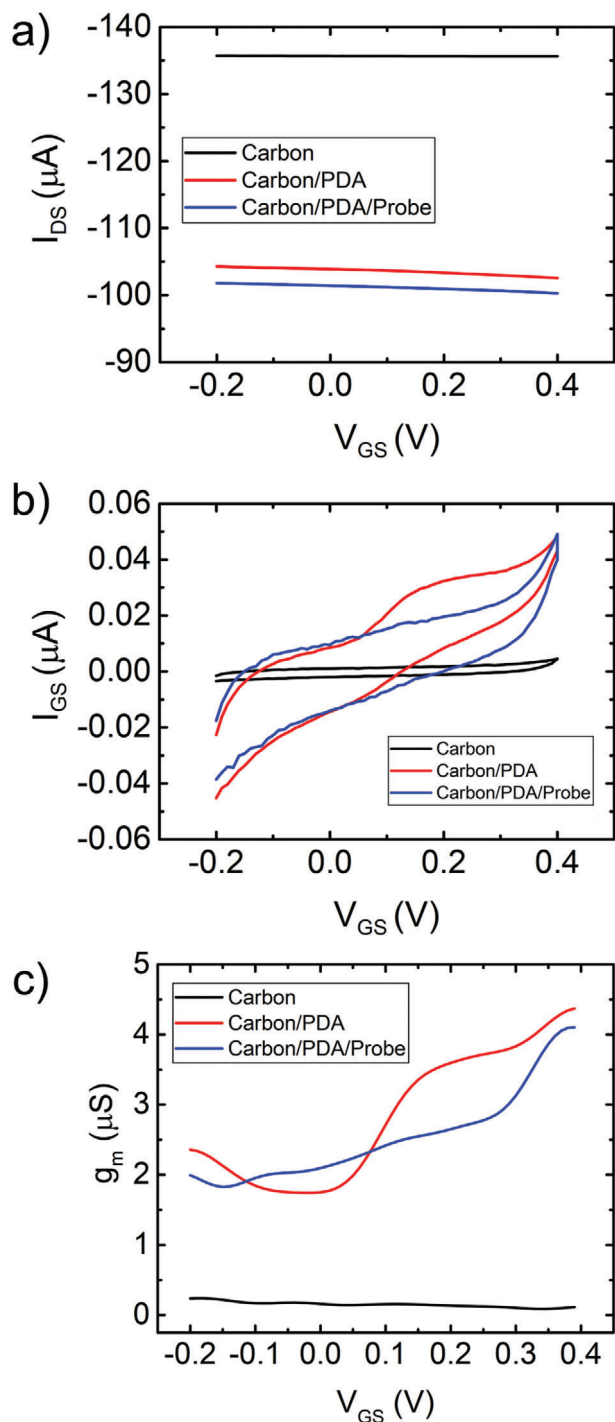


Figure 2. Probe DNA immobilization on the gate. a) I_{DS} and b) I_{GS} versus V_{GS} curves of the OECT recorded after each step of functionalization of the gate at $V_{DS} = -0.2$ V. c) Transconductance (g_m) extracted from the data in panel a) by calculating the first derivative of the curves. All measurements have been performed in PBS 1 \times , at pH 7.4.

-0.2 V were applied. The gate-source voltage window was chosen to avoid further redox processes within the PDA film^[28] (see Figure S2, Supporting Information); moreover, the sweeping of the V_{GS} during the hybridization was adopted since it was suggested that DNA hybridization could be facilitated by sweeping the potential applied to an electrode modified with the DNA probe.^[42] As shown in Figure 3a, upon exposure to 1×10^{-12} M of fc-target, the I_{DS} current increases, and the transfer curve is shifted to higher potentials. This trend was observed before in OECT operated as DNA biosensors.^[21] PEDOT:PSS based OECTs operate in depletion mode, i.e., a positive voltage is required to induce the penetration of cations in the polymer film (channel), which leads to a decrease in the current in the channel. We might ascribe the current increase upon target hybridization to the negative charge of the oligonucleotides, mostly contributed by the phosphate groups, which cause a larger voltage drop at the gate-electrolyte interface; as a consequence, the device responds as a less positive gate potential was applied.

As shown in Figure 3a, the current increases monotonically up to 100×10^{-9} M, although the smaller increase at the higher concentration values suggests a saturation of the probes on the gate. To quantitatively monitor the hybridization process, we extracted from the current data a response signal (S), calculated as $S = \Delta I / I_0$, where I_0 is the I_{DS} of the same device measured in the PBS buffer ($[fc\text{-target}] = 0$ M in Figure 3a) at a specific V_{GS} , while ΔI is equal to the difference between the I_{DS} at a specific analyte concentration and I_0 , both at the same V_{GS} .

In Figure 3b the signal S obtained at $V_{GS} = +0.4$ V, which is the potential of maximum transconductance, is shown as the average of $n = 4$ independent devices, whose error bars represent the standard deviation. The obtained signal was below 10%, which is lower than what we observed with EGOT biosensors for protein^[5] and viruses,^[11] where values up to 60% were recorded. This is probably to be ascribed to the fact that the current modulation in the investigated range is limited, as further confirmed by the very small differences observed for the signal dependence on the V_{GS} at which the values are extracted (see Figure S3, Supporting Information). Nevertheless, the device response can be unambiguously ascribed to the DNA hybridization, as confirmed by control experiments (vide infra and Figure S6, Supporting Information). The signal S increases linearly with the logarithm of the target concentration and tends to a plateau for $[fc\text{-target}]$ equal to or higher than 1×10^{-9} M. We calculated a theoretical limit of detection (LOD) of $\approx 100 \times 10^{-15}$ M, by adding to the current when $[fc\text{-target}] = 0$ M the standard deviation multiplied by 3. As recently proposed by our group,^[45] we fit the Frumkin isotherm to the dose curve to gain insight into the thermodynamics of fc-target/probe hybridization. To this end, we first calculated the surface coverage $\theta = S / S_{max}$ by assuming S_{max} to be 5% higher than the highest observed S value. We then plotted (Figure 3c) $\ln[fc\text{-target}]$ versus θ and fit our data using the following equation by recasting the Frumkin isotherm:

$$\ln [fc\text{-Target}] = \ln K_a + \ln \theta - \ln (1 - \theta) - g' \theta \quad (1)$$

where K_a is the equilibrium probe/target association constant, and the Frumkin factor g' considers attractive (if positive) or repulsive (if negative) lateral interactions between probe/target pairs. The fit of Equation 1 to the dose curve, shown as the red

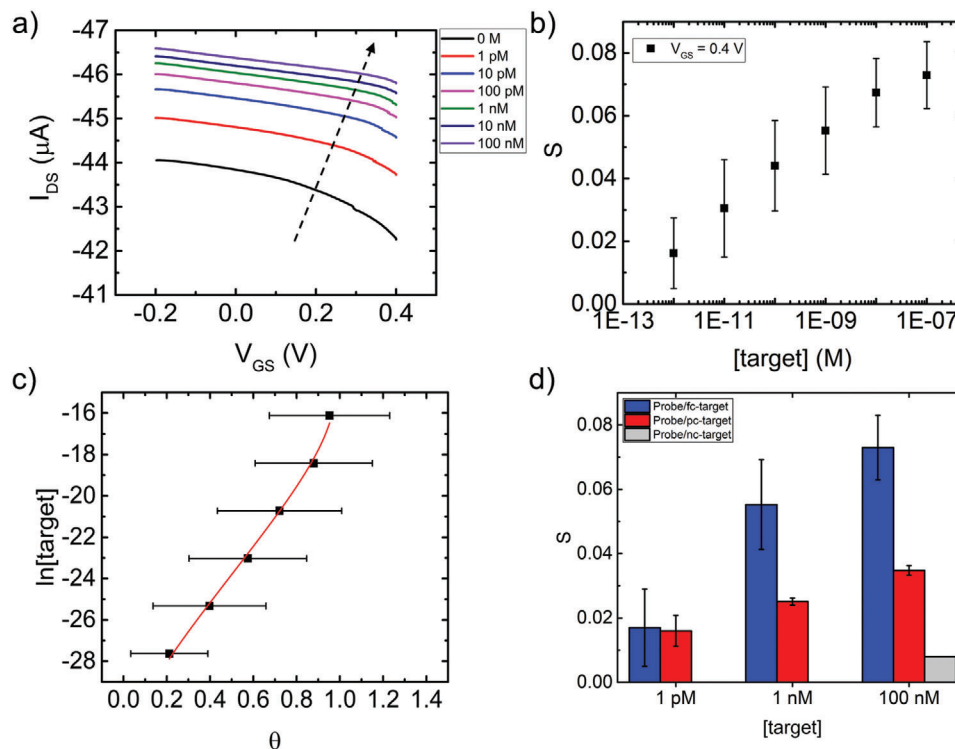


Figure 3. Target detection. a) Typical response of the OECT gated by a PDA-modified carbon gate upon exposure to increasing concentrations of fc-target DNA, recorded in PBS 1X, pH 7.4, at $V_{DS} = -0.2$ V. b) Semilog plot of the device response S as a function of [fc-target]. The error bars are the SD resulting from the measurement of four independent devices (3 for 10×10^{-3} and 100×10^{-3} M). c) $\ln[\text{fc-target}]$ versus θ plot. The red line has been obtained by fitting Equation 1 to the data. The error bars are the result of error propagation. d) Response of the device to fc-target (blue bars), pc-target (red bars) and nc-target (grey bar) at 1×10^{-12} , 1×10^{-9} , and 100×10^{-9} M, respectively.

curve in Figure 3c, yields $K_a = 2.6 \times 10^{12} \pm 7.8 \times 10^{11}$, and $g' = -9.6 \pm 0.4$, the latter value indicating repulsions between negatively charged dsDNA that forms on the gate surface. From the K_a values, we readily obtain the standard free energy change $\Delta G^\circ = -71$ kJ mol $^{-1}$ for the hybridization between the surface-bound probe and the freely diffusing target.

We also performed a set of control experiments to verify the specificity of the biosensor toward the complementary strand. To assess the ability of the device to specifically detect the complementary strand, we exposed the device functionalized with the probe to a non-complementary oligonucleotide (nc-target hereafter), for which DINAMelt^[47] predicted annealing of a maximum of five bases out of 25 (the annealed sequences are shown in Figure S4, Supporting Information). We tested the response to the nc-target at the highest concentration investigated for the fc-target (namely 100×10^{-9} M). As shown by the histograms in Figure 3d, the response to nc-target at 100×10^{-9} M concentration yields a signal that is approximately tenfold lower than the signal generated by the same concentration of fc-target.

As a further control, we measured the biosensor upon exposure to an oligonucleotide which is only partially complementary to the surface-bound probe (pc-target hereafter), as it bears five mismatches. For pc-target, we recorded the response at 1×10^{-12} , 1×10^{-9} , and 100×10^{-9} M. The signal S for pc-target is comparable to that for fc-target at 1×10^{-12} M concentration, while the signal at 1×10^{-9} and 100×10^{-9} M is about twofold lower for pc-target than for fc-target. These results suggest that, as ex-

pected, the pc-target DNA can bind to the probe despite the mismatches, as it still bears large regions of complementary residues that might ensure hybridization. Noticeably, the device cannot discriminate between the two strands at the lowest concentration, while the significant difference for S at 1×10^{-9} and 100×10^{-9} M indicates that pc-target binds with lower affinity, hence a smaller association constant, allowing discrimination between fc-target and pc-target.

This confirms that, despite the OECT response inferior to that of state-of-the-art reported OECT devices, the signal variation is significant and can be safely used to discriminate between fully complementary sequences and partially mismatched sequences with differences of only a few bases.

Furthermore, the performances of the genosensor, in terms of specificity, limit of detection ($\approx 100 \times 10^{-15}$ M), time required for the measurement (15 min), and dynamic range (4 orders of magnitude) are comparable with genosensors in literature based on surface plasmon resonance^[48] and electrochemical methods.^[49] Compared to most of the devices based on SPR and Electrochemical methods, our genosensor has properties that make it more prompt to point of care applications; substrate flexibility, ease of use, cost-effectiveness, and fast response.

3. Conclusion

In this work, we demonstrated the first example of an OECT biosensor where the probe is immobilized on the gate by means

of a bio-based and bioinspired PDA film deposited by drop-casting. We showed that thanks to the PDA film, the gate can be easily functionalized with amine-modified single-stranded DNA by simple incubation. In principle, this strategy can be readily adapted to any protein or molecule of interest presenting the respective amine or thiol groups. The presented OECT genosensor was able to detect a fully complementary oligonucleotide, showing a theoretical LOD of $\approx 100 \times 10^{-15}$ M and a dynamic range from 1×10^{-12} to 10×10^{-9} M. Furthermore, the different responses of the device toward partially complementary and non-complementary strands compared to the fully complementary one showed that the response of the device is clearly correlated with the hybridization process between the strands.

From a perspective, the functional immobilization of a DNA probe on an OECT biosensor may represent a new tool to quantify the levels of a DNA-binding factor, such as NF- κ B, which has been proposed as a biomarker predicting risk assessment of patients.^[38]

4. Experimental Section

Reagents: All chemical reagents were purchased from Sigma–Aldrich. The PBS 1x solution contained Na_2HPO_4 (10×10^{-3} M), KH_2PO_4 (1.8×10^{-3} M), KCl (2.7×10^{-3} M), and NaCl (137×10^{-3} M).

OECT Fabrication: The OECTs were manufactured by screen-printing techniques on PET (Polyfoil Bias; thickness = 125 μm) as previously described.^[17] A commercial Ag ink (Ag5000, DuPont, U.K.) was used to print the conductive tracks; the carbon gate and the carbon contact pads were printed using a commercial carbon ink (C2130307D1, Gwent, U.K.), while the channel of the device was obtained by printing a PEDOT:PSS commercial ink (Clevios SV3, Heraeus Group, Germany). Finally, an Ag/AgCl electrode was deposited using a commercial ink (C61003P7, Gwent/Sun Chemical).

By coating with a dielectric layer (5018, DuPont, UK), only the gate, the channel, and the final contacts of the conductive tracks were left exposed. All of the devices used in this work had the geometry described in the following paragraph. The area of the gate was 2 mm², while the channel had a dimension of 2×3 mm². The channel thickness, as determined by atomic force microscopy, was 280 ± 20 nm. Gate and channel were placed at a distance of 2 mm; this was introduced to ensure the easy and selective modification of the gate by means of drop-casting. The OECT was printed by using a semi-automatic screen printer (DEK Horizon 03i printer, ASM Assembly Systems GmbH, Germany).

The gate was functionalized as described previously in the text.

Electrical Characterization: The transfer curves were measured at room temperature by means of an Agilent B2902A Source Measure Unit (SMU), by fixing the V_{DS} at -0.2 V and sweeping the gate-source voltage between -0.2 V and 0.4 V. The electrolyte consisted in a 40 μL drop of PBS (1x, pH 7.4) that covered both the gate and channel surfaces.

Electrochemical Characterization: The electrochemical measurements, in a three electrodes configuration, were performed with a CH Instruments potentiostat 760c by connecting the gate as the working electrode. An Ag/AgCl electrode (reference electrode), also printed on the device, and a platinum wire (counter electrode) were used to complete the electrochemical cell. Measurements were performed by immersing the electrodes in a drop of the electrolyte solution. The CVs were recorded by sweeping the potential between -0.1 V and 0.4 V, at 50 mV s⁻¹, in PBS (1x, at pH 7.4). The EIS measurements were performed with the same setup but with a drop of $\text{K}_3\text{Fe}(\text{CN})_6$ (5×10^{-3} M) and KCl (0.1 M). The potential was set to 0.2 V, with an amplitude of 10 mV and in the range of frequencies from 0.1 Hz to 100 kHz.

Oligonucleotides: The oligonucleotides were purchased from IDT.

Oligonucleotides sequences:

- probe: 5'-/AmMC6/TTC TGA GCC AAT CAC CGA GCT CGA T-3'
- fc-target: 5'-ATC GAG CTC GGT GAT TGG CTC AGA A-3'
- pc-target: 5'-ATC GAG CTC GGT GGC CAA CTC AGA A-3'
- nc-target: 5'-GGT TGG GAA TTG CAA CAT GGT TCG ATT GCG AGC CCA-3'

Supporting Information

Supporting Information is available from the Wiley Online Library or from the author.

Acknowledgements

This work was funded by the EuroNanoMed III project “AMI”. M.S. was supported by Fondazione Umberto Veronesi. The authors would like to thank Ms. Marie Nillson and Ms. Kathrin Hübscher for the screen-printing of the OECTs. V.B. was supported by the Swedish Foundation for Strategic Research (Smart Intra-body network; grant RIT15-0119). This project received funding from the European Union’s Horizon 2020 research and innovation program under the Marie Skłodowska-Curie grant agreement no. 813863. The laboratory of C.I. was supported by AIRC IG 2018 – ID. 21323 project.

Open Access Funding provided by Università degli Studi di Modena e Reggio Emilia within the CRUI-CARE Agreement.

Conflict of Interest

The authors declare no conflict of interest.

Data Availability Statement

The data that support the findings of this study are openly available in Zenodo at <http://doi.org/10.5281/zenodo.5884277>.

Keywords

genosensors, OECTs, organic electronics, polydopamine

Received: November 24, 2021

Revised: January 22, 2022

Published online: February 10, 2022

- [1] A.-M. Pappa, O. Parlak, G. Scheiblin, P. Mailley, A. Salleo, R. M. Owens, *Trends Biotechnol.* **2018**, 36, 45.
- [2] S. Casalini, F. Leonardi, T. Cramer, F. Biscarini, *Org. Electron. physics, Mater. Appl.* **2013**, 14, 156.
- [3] I. Gualandi, D. Tonelli, F. Mariani, E. Scavetta, M. Marzocchi, B. Fraboni, *Sci. Rep.* **2016**, 6, 33637.
- [4] L. Zhang, G. Wang, C. Xiong, L. Zheng, J. He, Y. Ding, H. Lu, G. Zhang, K. Cho, L. Qiu, *Biosens. Bioelectron.* **2018**, 105, 12.
- [5] M. Berto, S. Casalini, M. Di Lauro, S. L. Marasso, M. Cocuzza, D. Perrone, M. Pinti, A. Cossarizza, C. F. Pirri, D. T. Simon, M. Berggren, F. Zerbetto, C. A. Bortolotti, F. Biscarini, *Anal. Chem.* **2016**, 88, 12330.
- [6] E. Macchia, K. Manoli, B. Holzer, C. Di Franco, M. Ghittorelli, F. Torricelli, D. Alberga, G. F. Mangiatordi, G. Palazzo, G. Scamarcio, L. Torsi, *Nat. Commun.* **2018**, 9, 3223.

- [7] K. Guo, S. Wustoni, A. Koklu, E. Díaz-Galicia, M. Moser, A. Hama, A. A. Alqahtani, A. N. Ahmad, F. S. Alhamlan, M. Shuaib, A. Pain, I. McCulloch, S. T. Arold, R. Grünberg, S. Inal, *Nat. Biomed. Eng.* **2021**, 5, 666.
- [8] M. Sensi, M. Berto, S. Gentile, M. Pinti, A. Conti, G. Pellacani, C. Salvarani, A. Cossarizza, C. A. Bortolotti, F. Biscarini, *Chem. Commun.* **2021**, 57, 367.
- [9] P. Lin, X. Luo, I.-M. Hsing, F. Yan, *Adv. Mater.* **2011**, 23, 4035.
- [10] M. Selvaraj, P. Greco, M. Sensi, G. D. Saygin, N. Bellassai, R. D'agata, G. Spoto, F. Biscarini, *Biosens. Bioelectron.* **2021**, 182, 113144.
- [11] M. Berto, E. Vecchi, L. Baiamonte, C. Condò, M. Sensi, M. Di Lauro, M. Sola, A. De Stradis, F. Biscarini, A. Minafra, C. A. Bortolotti, *Sensors Actuators B Chem* **2019**, 281, 150.
- [12] G. Tarabella, C. Santato, S. Y. Yang, S. Iannotta, G. G. Malliaras, F. Cicoira, *Appl. Phys. Lett.* **2010**, 97, 123304.
- [13] M. Sensi, M. Berto, A. Candini, A. Liscio, A. Cossarizza, V. Beni, F. Biscarini, C. A. Bortolotti, *ACS Omega* **2019**, 4, 5374.
- [14] C. Diacci, T. Abedi, J. Lee, E. O. Gabrielsson, M. Berggren, D. T. Simon, T. Niittylä, E. Stavrinidou, *iScience* **2020**, 24, 101966.
- [15] D. A. Koutsouras, F. Torricelli, P. Gkoupidenis, P. W. M. Blom, *Adv. Mater. Technol.* **2021**, 6, 2100732.
- [16] M. Galliani, C. Diacci, M. Berto, M. Sensi, V. Beni, M. Berggren, M. Borsari, D. T. Simon, F. Biscarini, C. A. Bortolotti, *Adv. Mater. Interfaces* **2020**, 7, 2001218.
- [17] M. Berto, C. Diacci, L. Theuer, M. Di Lauro, D. T. Simon, M. Berggren, F. Biscarini, V. Beni, C. A. Bortolotti, *Flex. Print. Electron.* **2018**, 3, 024001.
- [18] M. Zabhipour, R. Lassnig, J. Strandberg, M. Berggren, S. Fabiano, I. Engquist, P. Andersson Ersman, *npj Flex. Electron.* **2020**, 4, 15.
- [19] P. Andersson Ersman, R. Lassnig, J. Strandberg, D. Tu, V. Keshmiri, R. Forchheimer, S. Fabiano, G. Gustafsson, M. Berggren, *Nat. Commun.* **2019**, 10, 5053.
- [20] W. Tao, P. Lin, J. Hu, S. Ke, J. Song, X. Zeng, *RSC Adv.* **2017**, 7, 52118.
- [21] J. Peng, T. He, Y. Sun, Y. Liu, Q. Cao, Q. Wang, H. Tang, *Microchim. Acta* **2018**, 185, 408.
- [22] L. Kergoat, B. Piro, M. Berggren, M.-C. Pham, A. Yassar, G. Horowitz, *Org. Electron.* **2012**, 13, 1.
- [23] E. Macchia, K. Manoli, C. Di Franco, R. A. Picca, R. Österbacka, G. Palazzo, F. Torricelli, G. Scamarcio, L. Torsi, *ACS Sens.* **2020**, 5, 1822.
- [24] S. Casalini, C. A. Bortolotti, F. Leonardi, F. Biscarini, *Chem. Soc. Rev.* **2017**, 46, 40.
- [25] J. Pallu, M. Avci-Adali, P. Mackeben, L. Mohammadnejad, G. Mattana, V. Noël, B. Piro, *Org. Electron.* **2019**, 75, 105402.
- [26] H. Tang, P. Lin, H. L. W. Chan, F. Yan, *Biosens. Bioelectron.* **2011**, 26, 4559.
- [27] S. Casalini, A. C. Dumitru, F. Leonardi, C. A. Bortolotti, E. T. Herruzo, A. Campana, R. F. De Oliveira, T. Cramer, R. Garcia, F. Biscarini, *ACS Nano* **2015**, 9, 5051.
- [28] P. Palladino, F. Bettazzi, S. Scarano, *Anal. Bioanal. Chem.* **2019**, 411, 4327.
- [29] H. Lee, S. M. Dellatore, W. M. Miller, P. B. Messersmith, *Science* **2007**, 318, 426.
- [30] J. H. Ryu, P. B. Messersmith, H. Lee, *ACS Appl. Mater. Interfaces* **2018**, 10, 7523.
- [31] Q. Lyu, N. Hsueh, C. L. L. Chai, *Polym. Chem.* **2019**, 10, 5771.
- [32] H. Lee, J. Rho, P. B. Messersmith, *Adv. Mater.* **2009**, 21, 431.
- [33] Y. Meng, P. Liu, W. Zhou, J. Ding, J. Liu, *ACS Nano* **2018**, 12, 9070.
- [34] P. Kanyong, S. Rawlinson, J. Davis, *Sensors Actuators B Chem.* **2016**, 233, 528.
- [35] A. Sukeri, A. Arjunan, M. Bertotti, *Electrochem. Commun.* **2020**, 110, 106622.
- [36] M. E. Lynge, R. Van Der Westen, A. Postma, B. Städler, *Nanoscale* **2011**, 3, 4916.
- [37] G. Wang, Q. Xu, L. Liu, X. Su, J. Lin, G. Xu, X. Luo, *ACS Appl. Mater. Interfaces* **2017**, 9, 31153.
- [38] A. Gurtner, I. Manni, G. Piaggio, *Biochim. Biophys. Acta – Gene Regul. Mech.* **2017**, 1860, 604.
- [39] S. Belluti, V. Semeghini, G. Rigillo, M. Ronzio, D. Benati, F. Torricelli, L. Reggiani Bonetti, G. Carnevale, G. Grisendi, A. Ciarrocchi, M. Dominici, A. Recchia, D. Dolfini, C. Imbriano, *J. Exp. Clin. Cancer Res.* **2021**, 40, 362.
- [40] Y. Zhang, X. Geng, J. Ai, Q. Gao, H. Qi, C. Zhang, *Sensors Actuators B Chem.* **2015**, 221, 1535.
- [41] T. Marchesi D'Alvise, S. Harvey, L. Hueske, J. Szelwicka, L. Veith, T. P. J. Knowles, D. Kubiczek, C. Flaig, F. Port, K. E. Gottschalk, F. Rosenau, B. Graczykowski, G. Fytas, F. S. Ruggeri, K. Wunderlich, T. Weil, *Adv. Funct. Mater.* **2020**, 30, 2000378.
- [42] M. Amiri, E. Amali, A. Nematollahzadeh, *Sensors Actuators B Chem.* **2015**, 216, 551.
- [43] J. Liebscher, *European J. Org. Chem.* **2019**, 2019, 4976.
- [44] J. Tymoczko, W. Schuhmann, M. Gebala, *ACS Appl. Mater. Interfaces* **2014**, 6, 21851.
- [45] P. A. Manco Urbina, M. Berto, P. Greco, M. Sensi, S. Borghi, M. Borsari, C. A. Bortolotti, F. Biscarini, *J. Mater. Chem. C* **2021**, 9, 10965.
- [46] S. Demuru, C. H. Huang, K. Parvez, R. Worsley, G. Mattana, B. Piro, V. Noël, C. Casiraghi, D. Briand, *ACS Appl. Nano Mater* **2022**, 5, 1664.
- [47] N. R. Markham, M. Zuker, *Nucleic Acids Res.* **2005**, 33, W577.
- [48] A. Bonyár, *ACS Appl. Nano Mater* **2020**, 3, 8506.
- [49] E. O. Blair, D. K. Corrigan, *Biosens. Bioelectron.* **2019**, 134, 57.